Inorganic Chemistry
Article

Inorg. Chem. **2010**, *49*, 5977–5985 **5977**
DOI: 10.1021/ic100502x

Mechanistic Study of Amine to Imine Oxidation in a Dinuclear Cu(II) Complex Containing an Octaaza Dinucleating Ligand

Gemma J. Christian,[†] Antoni Llobet,[†,‡] and Feliu Maseras*[,†,‡]

[†]*Institute of Chemical Research of Catalonia (ICIQ), Avinguda Països Catalans 16, 43007 Tarragona, Catalonia, Spain, and* [‡]*Departament de Química, Universitat Autònoma de Barcelona, 08193 Bellaterra, Catalonia, Spain*

Received March 16, 2010

Density functional theory (DFT) calculations have been carried out to elucidate the mechanism of self-oxidation of a Cu(II) complex octaaza dinucleating macrocyclic ligand. The reaction is bimolecular and spontaneous, in which amine groups of one macrocycle are oxidized and the Cu^{II} centers of a second macrocylic complex are reduced. No additional oxidation or external base agents are required. DFT calculations predict the reaction to proceed via a two-step mechanism, in which the first step is proton transfer between two reactant complexes. This is followed by a second transfer step in which an electron and proton are transferred together between the two complexes. Concurrent with this external transfer there is also an internal electron transfer in which the ligand reduces the metal center to give the imine product bound to Cu^{I}. The complexity of this final step differs from the generally accepted mechanisms for transition metal catalyzed amine to imine oxidation in which protons and electrons are transferred individually.

Introduction

Macrocyclic ligands are a growing class of compounds because of their diverse nature and multiple applications.[1,2] Within this field we[3] have recently developed a family of macrocyclic ligands based on hexaaza and octaaza binding groups that are summarized in Figure 1.

All these macrocyclic ligands react with Cu(I) or Cu(II) to generate the corresponding dinuclear complexes. The electronic and geometric properties of these dinuclear complexes are fine-tuned by the combination of effects exerted by the macrocyclic ligands, namely, (a) the *para* or *meta* substitution in the aromatic spacer, (b) the two or three methylenic units in the aminic or iminic arms, (c) the secondary or tertiary nature of the amine, and (d) the presence or absence of additional coordinating pendant arms.[4] In addition, the macrocyclic ligands also make it possible to control the relative disposition of the two metal centers and thus can generate genuine cooperative effects for DNA interactions,[5] for the recognition of anions,[6] and for the activation of small molecules such as dioxygen,[7] carbon dioxide, and so forth.[8]

Among all dinuclear Cu(II) complexes containing the macrocyclic ligands represented in Figure 1, only the octaaza shown in Figure 2, $[H_4LCu^{II}_2]^{4+}$, (L has *para* substitution, 3 methylenic units, and a 2(methyl)pyridyl pendant arm)

*To whom correspondence should be addressed. E-mail: fmaseras@iciq.es.

(1) (a) Matano, Y.; Miyajima, T.; Ochi, N.; Nakabuchi, T.; Shiro, M.; Nakao, Y.; Sakaki, S.; Imahori, H. *J. Am. Chem. Soc.* **2008**, *130*, 990–1002. (b) Busch, D. H. *Acc. Chem. Res.* **1978**, *11*, 392–400. (c) Alexander, V. *Chem. Rev.* **1995**, *95*, 273–342.

(2) (a) Bencini, A.; Bianchi, A.; Scott, E. C.; Morales, M.; Wang, B.; Garcia-España, E.; Deffo, T.; Takusagawa, F.; Mertes, M. P.; Mertes, K.-B.; Paoletti, P. *Bioorg. Chem.* **1992**, *20*, 8–29. (b) Izatt, R. M.; Pawlak, K.; Bruening, R. L. *Chem. Rev.* **1995**, *95*, 2529–2586. (c) Formica, M.; Fusi, V.; Micheloni, M.; Pontellini, R.; Romani, P. *Coord. Chem. Rev.* **1999**, *184*, 347–363. (d) Sun, X.; Wuest, M.; Weisman, G. R.; Wong, E. H.; Reed, D. P.; Boswell, C. A.; Motekaitis, R.; Martell, A. E.; Welch, M. J.; Anderson, C. J. *J. Med. Chem.* **2002**, *45*, 469–477.

(3) (a) Costas, M.; Xifra, R.; Llobet, A.; Solà M., M.; Robles, J.; Parella, T.; Stoeckli-Evans, H.; Neuburger, M. *Inorg. Chem.* **2003**, *42*, 4456–4468. (b) Costas, M.; Anda, C.; Llobet, A.; Parella, T.; Evans, H. S.; Pinilla, E. *Eur. J. Inorg. Chem.* **2004**, 857–865. (c) Anda, C.; Martinez, M. A.; Llobet, A. *Supramol. Chem.* **2005**, *17*, 257–266. (d) Company, A.; Lamata, D.; Poater, A.; Solà, M.; Rybak-Akimova, E. V.; Que, L.; Fontrodona, X.; Parella, T.; Llobet, A.; Costas, M. *Inorg. Chem.* **2006**, *45*, 5239–5241.

(4) Costas, M.; Ribas, X.; Poater, A.; López Valbuena, J. M.; Xifra, R.; Company, A.; Duran, M.; Solà, M.; Llobet, A.; Corbella, M.; Uson, M. A.; Mahia, J.; Solans, X.; Shan, X.; Benet-Buchholz, J. *Inorg. Chem.* **2006**, *45*, 3569–3581.

(5) Arbuse, A.; Font, M.; Martínez, M. A.; Fontrodona, X.; Prieto, M. J.; Moreno, V.; Sala, X.; Llobet, A. *Inorg. Chem.* **2009**, *48*, 11098–11107.

(6) (a) Anda, C.; Llobet, A.; Salvado, V.; Motekaitis, R.; Riebenspies, J.; Martell, A. E. *Inorg. Chem.* **2000**, *39*, 2986–2999. (b) Anda, C.; Llobet, A.; Salvado, V.; Motekaitis, R.; Martell, A. E. *Inorg. Chem.* **2000**, *39*, 3000–3008. (c) Anda, C.; Llobet, A.; Martell, A. E.; Donnadieu, B.; Parella, T. *Inorg. Chem.* **2003**, *42*, 8545–8550. (d) Anda, C.; Llobet, A.; Martell, A. E.; Riebenspies, J.; Berni, E.; Solans, X. *Inorg. Chem.* **2004**, *43*, 2793–2802. (e) Arbuse, A.; Anda, C.; Martínez, M. A.; Perez-Mirón, J.; Jaime, C.; Parella, T.; Llobet, A. *Inorg. Chem.* **2007**, *46*, 10632–10638.

(7) Poater, A.; Ribas, X.; Cavallo, L.; Llobet, A.; Solà, M. *J. Am. Chem. Soc.* **2008**, *130*, 1770–1771.

(8) Company, A.; Jee, J. E.; Ribas, X.; López-Valbuena, J. M.; Gómez, L.; Corbella, M.; Llobet, A.; Mahia, J.; Benet-Buchholz, J.; Costas, M.; van Eldik, R. *Inorg. Chem.* **2007**, *46*, 9098–9110.

Published on Web 06/10/2010

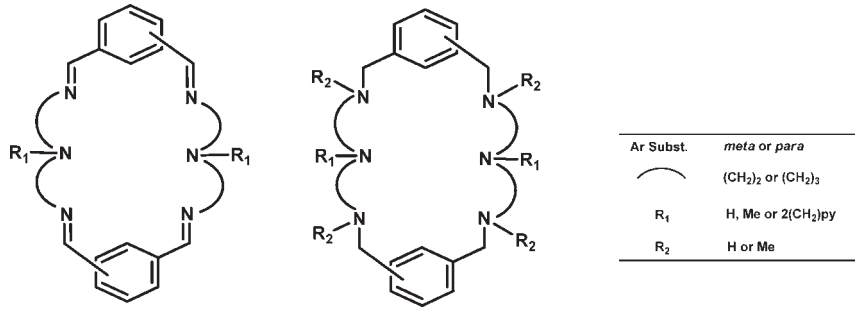

Figure 1. Macrocyclic ligands.

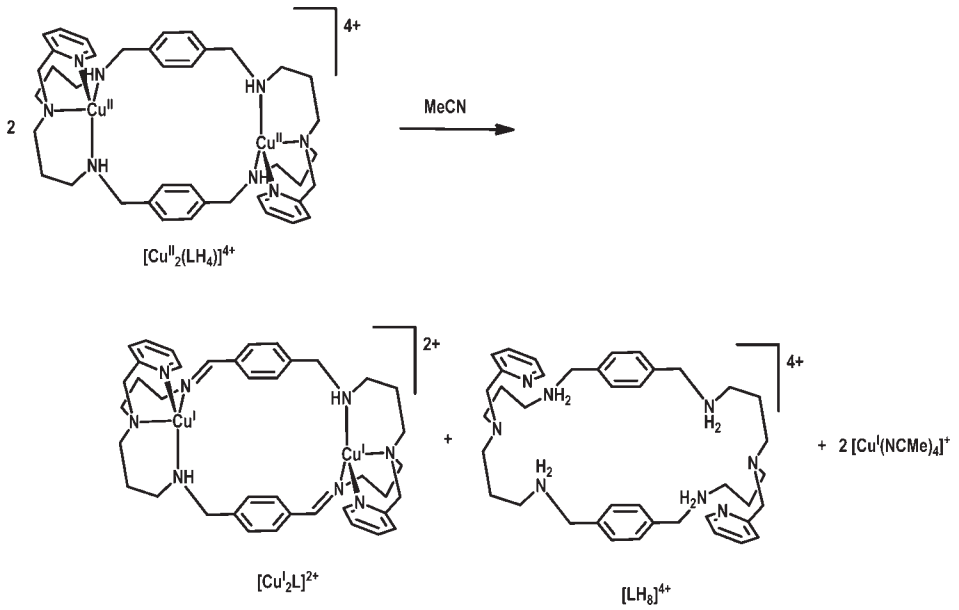

Figure 2. Amine to imine oxidation reaction for $[H_4LCu^{II}{}_2]^{4+}$.

undergoes a spontaneous self-oxidation−reduction reaction where Cu(II) is reduced to Cu(I), and half of the amine groups of the ligand are oxidized to the corresponding imines with a net loss of $2H^+$ and $2e^-$ (or 2 H-atoms) per N−C bond, and thus implicates a multi proton/electron redox process.

The uniqueness of this reaction that takes place only with L and in the absence of an added base is a consequence of the particular electronic properties exerted by the ligand to the Cu(II) center and vice versa. It is thus of interest to understand at a molecular level how and why this process occurs.

This reaction involves proton and electron transfers, and constitutes thus an example of these important types of processes that allow for the buildup of multiple redox equivalents needed to carry out multielectron reactions and provides low energy reaction pathways that avoid high energy intermediates. Multiple proton-coupled electron transfer (PCET) reactions[9] are being thoroughly studied because they are involved in a range of very important reactions, such as the oxidation of water to molecular oxygen[10] or the reduction of CO_2 to methanol.[11] Furthermore, nature also takes advantage of PCET in a variety of enzymatic processes, involving vitamin B_{12}, cytochromes P_{450}, lipoxygenases,[12] and in the activation of PSII toward water oxidation.[13]

There is little previous mechanistic work on amine oxidation by copper, although the process is known in both biological and synthetic systems.[14] The details at a molecular level are not well-understood yet,[15] thus further investigations are pertinent to mechanistically shed light on this important reaction. Within this context a mechanistic work involving an Fe(III) complex has been reported recently[16]

(9) (a) Huynh, M. H. V.; Meyer, T. *J. Chem. Rev*. **2007**, *107*, 5004–5064. (b) Hammes-Schiffer, S. *Acc. Chem. Res*. **2009**, *42*, 1881–1889. (c) Costentin, C.; Robert, M.; Saveant, J.-M. *Acc. Chem. Res*., in press, DOI:10.1021/ar9002812.

(10) (a) Romain, S.; Vigara, L.; Llobet, A. *Acc. Chem. Res*. **2009**, *42*, 1944–1953. (b) Romain, S.; Bozoglian, F.; Sala, X.; Llobet, A. *J. Am. Chem. Soc*. **2009**, *131*, 2768–2769.

(11) Morris, A. J.; Meyer, G. J.; Fujita, E. *Acc. Chem. Res*. **2009**, *42*, 1983–1994.

(12) Mayer, J. M. *Annu. Rev. Phys. Chem*. **2004**, *55*, 363–390.

(13) Meyer, T. J.; Huynh, M. H. V.; Thorp, H. H. *Angew. Chem., Int. Ed*. **2007**, *46*, 5284–5304.

(14) (a) Ridd, M. J.; Keene, F. R. . *J. Am. Chem. Soc*. **1981**, *103*, 5733–5740. (b) Keene, F. R.; Ridd, M. J.; Snow, M. R. *J. Am. Chem. Soc*. **1983**, *105*, 7075–7081. (c) Bernhard, P.; Sargeson, A. M. *J. Am. Chem. Soc*. **1989**, *111*, 597–606. (d) Murahashi, S. I.; Naota, T.; Taki, H. *J. Chem. Soc., Chem. Commun*. **1985**, 613–614. (e) Hipp, C. J.; Lindoy, L. F.; Busch, D. H. *Inorg. Chem*. **1972**, *11*, 1988–1994. (f) Goto, M.; Takeshita, M.; Kanda, N.; Sakai, T.; Goedken, V. L. *Inorg. Chem*. **1985**, *24*, 582–587. (g) Olson, D. C.; Vasilevskis, J. *Inorg. Chem*. **1971**, *10*, 463–470.

(15) (a) *Handbook on Metalloproteins*; Bertini, I., Sigel, A., Sigel, H., Eds.; Marcel Dekker: New York, 2001. (b) *Handbook of Metalloproteins*; Messerschmidt, A., Huber, R., Poulos, T., Wieghardt, K., Eds.; Wiley: Chichester, U.K., 2001.

(16) Saucedo-Vázquez, J. P.; Ugalde-Saldívar, V. M.; Toscano, A. R.; Kroneck, P. M. H.; Sosa-Torres, M. E. *Inorg. Chem*. **2009**, *48*, 1214–1222.

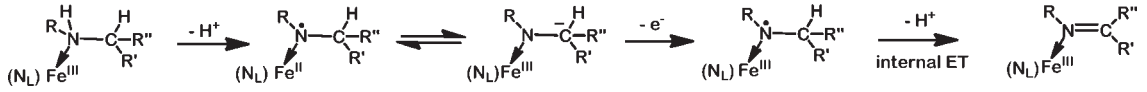

Figure 3. Amine to imine oxidation by transition metals.

whose main conclusions are summarized in Figure 3.[17] After an initial oxidation step a three step process is proposed involving (a) deprotonation of the ligand, (b) then electron transfer, and (c) a final deprotonation step to yield the imine.

The external electron transfer is carried out by the oxidized reactant available in the reaction mixture, while a second electron is transferred internally from the ligand to the metal during the second deprotonation. Thus, the overall reaction consists of the transfer of two protons from the amine to an external base, and the transfer of two electrons to the metal centers, one internal and one external, as shown in Figure 3. In contrast, in the reaction we analyze in the present paper no external base is required. We moreover showed in a previous study that electron transfer to the reactant is endothermic by 243 kJ mol^{-1}.[18] In the present study, density functional theory (DFT) is used to investigate in detail the mechanism of the copper catalyzed amine to imine oxidation reaction using a model system.

Computational Details and Model

DFT calculations were performed using the Gaussian 03 suite of programs[19] with the B3LYP* functional.[20] This functional differs from the commonly used B3LYP functional[21,22] in that it has 15% instead of 20% exact exchange and often better reproduces spin-state splittings in transition metal complexes,[23] although exceptions have been reported.[24] This functional was chosen to account for eventual nuances related to relative energies of spin states, although in the end it was not necessary, as in fact tests of critical structures on a smaller model for B3LYP, B3LYP*, BLYP[25,26] and BP[27] included in the Supporting Information find very similar results. All structures were optimized using the SDD basis set[28] for Cu and S while the 6-31G(d)[29,30] basis set was used for all remaining atoms. Final energies were calculated with a higher level basis set with SDD for Cu, and 6-31++G(d,p) for the remaining atoms with an additional d shell (exponent 0.503) for S. This is referred to as BS II in the text.

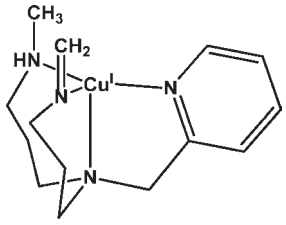

Figure 4. Mononuclear computational model of $[Cu^{II}_2(H_4L)]^{4+}$, shown here for the imine product $[Cu^{I}(L')]^{+}$.

Solvent effects for the model system were calculated using single-point polarizable continuum model (PCM)[31] calculations on gas phase geometries with acetonitrile as the solvent. UFF radii[32] were used for the construction of the cavity. This solvation model explicitly includes the solute hydrogen atoms in the cavity construction. Minima were confirmed through frequency calculations, and zero-point energy corrections are included for potential energies. Free energy corrections were also evaluated in the model calculations.

The complex was modeled by a mononuclear system with one copper center, shown in Figure 4. This model retains the coordination of the ligand to the metal center of the experimental system. The use of a mononuclear model is justified because the two Cu centers in the experimental system cannot interact to any significant degree as they are separated by over 7 Å with a relatively rigid linker between them. We are unable to envision a mechanism where at such a long distance the two copper centers in the same dinuclear system could be simultaneously invoved in the same redox step, and the introduction of the full system in the mechanistic study would be prohibitively expensive.

Cu^{II}, as a d^9 transition metal, generally forms five or six coordinate complexes.[33] Since the macrocycle binds to the metal via four donor atoms this leaves a vacant coordination site for some species along the reaction pathway. In crystal structures of similar systems this site is filled with the solvent or the counter-ion.[3] The solvent also plays an important role in the final step of the reaction where Cu^{I} dissociates and is coordinated by acetonitrile to form $[Cu^{I}(MeCN)_4]^{+}$. To correctly model the role of the solvent and the counter-ions, the binding of acetonitrile and/or the counter-ion, triflate, to the metal center was explored for each species along the reaction pathway, and they are included where they were found to be binding or to have a significant effect on the relative energies of the complexes. In the final product, four acetonitrile solvent molecules were included to allow for the formation of $[Cu^{I}(MeCN)_4]^{+}$. In all modeling the

(17) Goto, M.; Takeshita, M.; Kanda, N.; Sakai, T.; Goedken, V. L. *Inorg. Chem.* **1985**, *24*, 582–587.
(18) Christian, G. J.; Arbuse, A.; Fontrodona, X.; Martinez, M. A.; Llobet, A.; Maseras, F. *Dalton Trans.* **2009**, 6013–6020.
(19) Frisch, M. J.; Trucks, G. W.; Schlegel, H. B.; Scuseria, G. E.; Robb, M. A.; Cheeseman, J. R.; J. A. Montgomery, J.; T. Vreven, K. N. K.; Burant, J. C.; Millam, J. M.; Iyengar, S. S.; Tomasi, J.; Barone, V.; Mennucci, B.; Cossi, M.; Scalmani, G.; Rega, N.; Petersson, G. A.; Nakatsuji, H.; Hada, M.; Ehara, M.; Toyota, K.; Fukuda, R.; Hasegawa, J.; Ishida, M.; Nakajima, T.; Honda, Y.; Kitao, O.; Nakai, H.; Klene, M.; Li, X.; Knox, J. E.; Hratchian, H. P.; Cross, J. B.; Bakken, V.; Adamo, C.; Jaramillo, J.; Gomperts, R.; Stratmann, R. E.; Yazyev, O.; Austin, A. J.; Cammi, R.; Pomelli, C.; Ochterski, J. W.; Ayala, P. Y.; Morokuma, K.; Voth, G. A.; Salvador, P.; Dannenberg, J. J.; Zakrzewski, V. G.; Dapprich, S.; Daniels, A. D.; Strain, M. C.; Farkas, O.; Malick, D. K.; Rabuck, A. D.; Raghavachari, K.; Foresman, J. B.; Ortiz, J. V.; Cui, Q.; Baboul, A. G.; Clifford, S.; Cioslowski, J.; Stefanov, B. B.; Liu, G.; Liashenko, A.; Piskorz, P.; Komaromi, I.; Martin, R. L.; Fox, D. J.; Keith, T.; Al-Laham, M. A.; Peng, C. Y.; Nanayakkara, A.; Challacombe, M.; Gill, P. M. W.; Johnson, B.; Chen, W.; Wong, M. W.; Gonzalez, C.; Pople, J. A. *Gaussian 03*; Gaussian, Inc.: Wallingford, CT, 2004.
(20) Reiher, M.; Salomon, O.; Hess, B. A. *Theor. Chem. Acc.* **2001**, *107*, 48–55.
(21) Becke, A. D. *J. Chem. Phys.* **1993**, *98*, 5648–5652.
(22) Lee, C. T.; Yang, W. T.; Parr, R. G. *Phys. Rev. B* **1988**, *37*, 785–789.
(23) Harvey, J. N.; Aschi, M. *Faraday Discuss.* **2003**, *124*, 129–143.
(24) (a) Reiher, M. *Inorg. Chem.* **2002**, *41*, 6928–6935. (b) Güell, M.; Solà, M.; Swart, M. *Polyhedron* **2010**, *29*, 84–93.
(25) Becke, A. D. *Phys Rev A* **1988**, *38*, 3098–3100.
(26) Lee, C.; Yang, W.; Parr, R. G. *Phys. Rev. B* **1988**, *37*, 785–789.
(27) Perdew, J. P. *Phys. Rev. B* **1986**, *33*, 8822–8824.
(28) Andrae, D.; Häussermann, U.; Dolg, M.; Stoll, H.; Preuss, H. *Theor. Chim. Acta* **1990**, *77*, 123–141.
(29) Hehre, W. J.; Ditchfield, R.; Pople, J. A. *J. Chem. Phys.* **1972**, *56*, 2257–2261.
(30) Francl, M. M.; Hehre, W. J.; Binkley, J.; Gordon, M. S.; Defrees, D. J.; Pople, J. A. *J. Chem. Phys.* **1982**, *77*, 3654–3665.
(31) Miertus, S.; Scrocco, E.; Tomasi, J. *Chem. Phys.* **1981**, *55*, 117–129.
(32) Rappe, A. K.; Casewit, C. J.; Colwell, K. S.; Goddard, W. A.; Skiff, W. M. *J. Am. Chem. Soc.* **1992**, *114*, 10024–10035.
(33) Rorabacher, D. B. *Chem. Rev.* **2004**, *104*, 651–697.

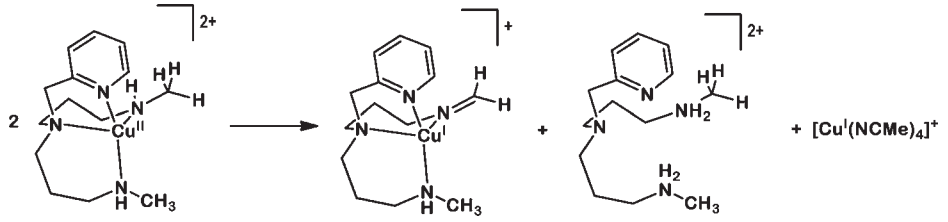

Figure 5. Amine to imine oxidation reaction shown in more detail for the model system.

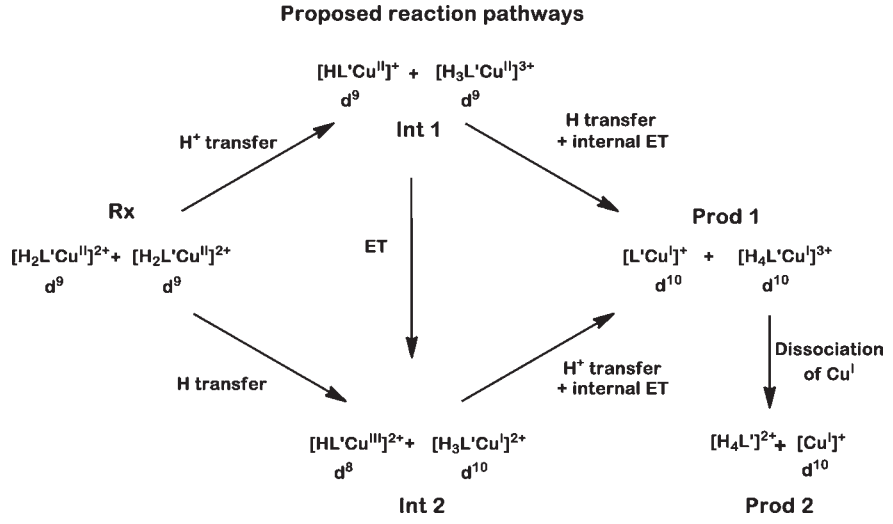

Figure 6. Proposed reaction pathways for the $2[H_2L'Cu^{II}]^{2+} \rightarrow [L'Cu^{I}]^{+} + H_4L'^{2+} + [Cu^{I}]^{+}$.

counter-ions were treated with DFT, as molecular mechanics treatment with MM charges was found to give unreliable results. The placement of the counter-ions was confirmed through systematic exploration of the possible conformations.

Scans to estimate barriers to proton and hydrogen transfer were carried out varying the relevant N−H distances. ONIOM calculations with the carbon atoms of the chelate rings in the MM region were used to preoptimize structures and then geometries were reoptimized with DFT for the highest energy points. Single point calculations with the higher basis set and solvent correction calculations were also carried out for the highest points of the scan. ZPE corrections were not applied for the large model used in the scan. Frequency calculations are expensive, and the neglect of this term is further justified because in the calculations on the mononuclear models (for example in Figure 7) the ZPE corrections were found to be small (8 and 14 kJ mol^{-1} for Int 1 and Int 2) and to stabilize the intermediates compared to reactants.

Results and Discussion

The overall amine to imine reaction observed experimentally is depicted in Figure 2 and written in a simplified manner in the following equation:

$$2[Cu^{II}{}_2(LH_4)]^{4+} + 8MeCN \rightarrow [Cu^{I}{}_2L]^{2+} + [LH_8]^{4+} + 2[Cu^{I}(MeCN)_4]^{+}$$

The reaction was explored using the mononuclear model shown in Figure 4. This model retains the coordination at the metal center of the experimental system. For the mononuclear model the experimental amine to imine reaction becomes

$$2[H_2L'Cu^{II}]^{2+} + 4MeCN \rightarrow [L'Cu^{I}]^{+} + H_4L'^{2+} + [Cu^{I}(MeCN)_4]^{+}$$

This is shown schematically in Figure 5. The amine to imine oxidation involves the loss of two electrons and two protons from the ligand. Two protons and one electron are transferred between the complexes, while the second electron transfer is internal where the ligand reduces the metal center to which it is bound. It is not clear from the experimental results whether the transfer of the protons and electron occurs in three discrete steps, or in concerted processes where one proton and electron are transferred together as a hydrogen atom or as proton coupled electron transfer, nor at which point the internal electron transfer occurs.

If we consider only the transfers between the complexes there are several possible two and three step pathways. The internal electron transfer step can then be determined by inspection of the electronic structure of the intermediates. Electron transfer in the first step, between reactants to give $[H_2L'Cu]^{+}$ and $[H_2L'Cu]^{3+}$, or the corresponding electron transfer in the final step of the reaction, was calculated to be highly unfavorable, giving intermediates 392 and 205 kJ mol^{-1} above the reactants, respectively, and so can be excluded. This leaves three remaining reaction pathways:

(1) (a) H^+ transfer, then (b) H transfer
(2) (a) H transfer, then (b) H^+ transfer
(3) (a) H^+ transfer, (b) e^- transfer between the complexes, and finally (c) H^+ transfer

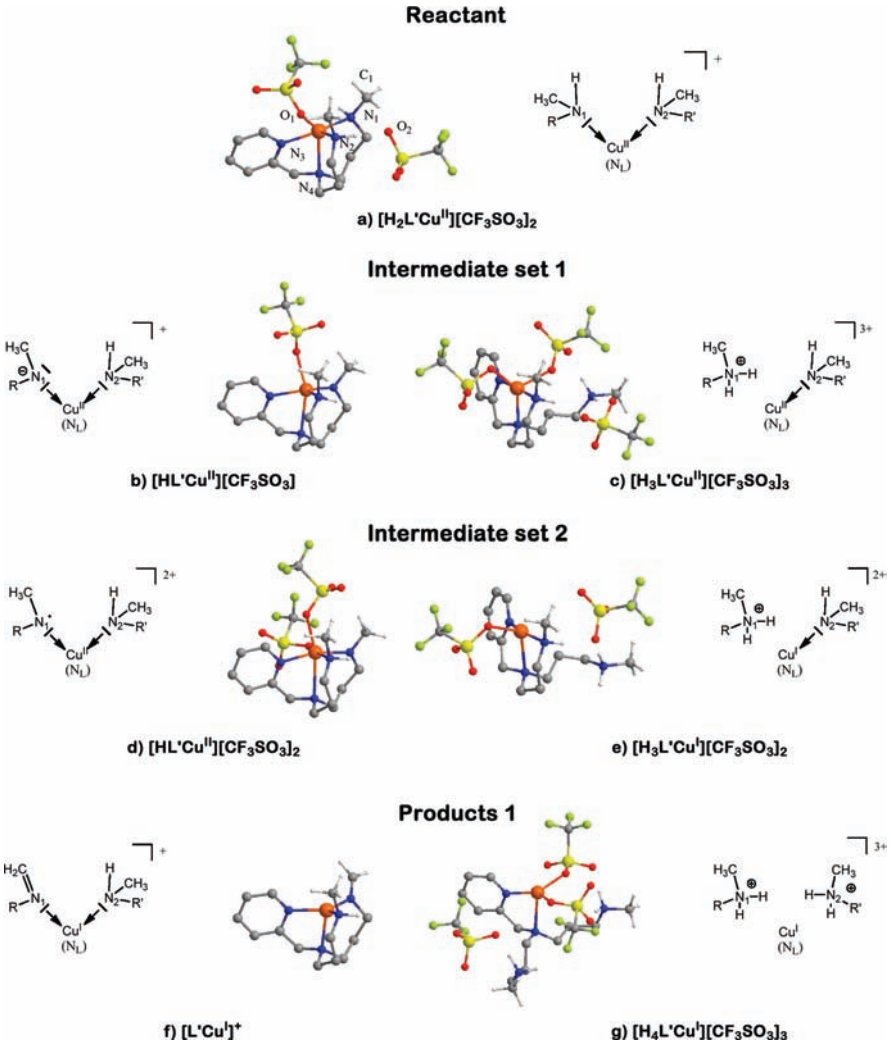

Figure 7. Optimized structures for species along the reaction pathway with schematic representation of the change in bonding between the copper centers and N donors N_1 and N_2. In these schemes N_L represents coordination to the rest of the ligand. Key hydrogen atoms are included in the optimized structures. The numbering scheme for the reactant has been used for all complexes..

For all three pathways the final step is dissociation of the protonated ligand to form the products.

These pathways can be inter-related as shown in Figure 6 since proton and then electron transfer, and hydrogen atom transfer give the same intermediates or products. Consequently there are only two sets of intermediates, labeled Intermediate set 1 (Int 1) and Intermediate set 2 (Int 2). Intermediate set 1 is made up of two d^9 copper complexes with charges of +1 and +3, and Intermediate set 2 is composed of a formally Cu^I and a formally Cu^{III} complex both with charges of +2. In this scheme, the internal electron transfer between the ligand and the copper center is proposed to occur during the formation of Products 1, but as mentioned above this must be confirmed by inspection of the electronic structure of the intermediates. Finally, the formation of the products has been artificially separated into Products 1 and Products 2, to observe the effect of protonation of the ligand and then its dissociation from the metal center.

The geometries and energies of the reactants, intermediates, and products were calculated for the model system, and optimized geometries are shown in Figure 7. The bonding situation with respect to the two amine donors is also represented schematically. Selected geometrical data are included in Table 1, and the calculated energies of the species along the reaction pathway are presented in Table 2.

Calculated Geometries. In the reactant, imine product and intermediates $[HL'Cu^{II}]^+$, and $[HL'Cu]^{2+}$, the ligand binds in a tetradentate manner, with the amine donor, N_4, in an apical position, and the Cu and remaining N donors form a rough plane. The shorter chelate arm of the pyridine ligand donor causes a tilting of the Cu−N_4 axis relative to the Cu−N plane. In all except the products, the coordination sphere of the copper center is completed by counter-ions. The products have Cu^I d^{10} metal centers and so after ligand binding there are no free coordination sites. The geometries of the reactant and products have been discussed in previous work and will not be discussed in detail here.[18]

Proton transfer between two reactant molecules gives Intermediate set 1. One of the molecules is deprotonated at N_1 to give $[HL'Cu^{II}]^+$ which has a formally d^9 copper center and a doublet ground state. The deprotonation is accompanied with a decrease in the C_1−N_1 bond length, attributable to the greater ionic character of the bond. The counter-ion moves from an axial position to a position approximately *trans* to the N_4 ligand donor, resulting

Table 1. Selected Bond Lengths (Å) for Reactants, Intermediates, and Products[a]

	C_1-N_1	$Cu-N_1$	$Cu-N_2$	$Cu-N_3$	$Cu-N_4$	$Cu-O_1$	$Cu-O_2$	$Cu-O_3$
				Reactant				
$[H_2L'Cu^{II}]^{2+}$	1.483	2.066	2.046	2.102	2.327	2.112	4.177	
				Int 1				
$[HL'Cu^{II}]^{+}$	1.455	1.898	2.177	2.101	2.526	2.264		
$[H_3L'Cu^{II}]^{3+}$	1.488	4.852	2.023	2.033	2.191	2.040	2.170	4.383
				Int 2				
$[HL'Cu^{II}]^{2+}$	1.442	2.029	2.225	2.041	2.586	2.025	2.218	
$[H_3L'Cu^{I}]^{2+}$	1.492	5.274	2.001	1.959	2.548	2.171	3.857	
				Products 1				
$[L'Cu^{I}]^{+}$	1.281 (1.277/1.288)	1.996 (1.984/1.975)	2.093 (2.058/2.046)	2.066 (2.058/2.051)	2.247 (2.211/2.204)			
$[H_4L'Cu^{I}]^{3+}$	1.487	4.205	5.493	1.969	2.476	2.033	2.067	4.708

[a] The numbering scheme is that of Figure 7. Available experimental values are included in parentheses.

Table 2. Calculated Energies of Reactants, Intermediate Sets 1 (Int 1) and 2 (Int 2), and Products 1 and 2 As Defined in Figure 6[a]

		ΔE (kJ/mol)	
	species	no counter-ions	counter-ions included
Rx	$2\,[H_2L'Cu^{II}]^{2+}$	0.0 (0.0)	0.0 (0.0)
Int 1	$[HL'Cu^{II}]^{+} + [H_3L'Cu^{II}]^{3+}$	76.8 (74.7)	18.6 (25.3)
Int 2	$[HL'Cu]^{2+} + [H_3L'Cu^{I}]^{2+}$	61.8 (57.1)	121.1 (134.6)
Prod 1	$[L'Cu^{I}]^{+} + [H_4L'Cu^{I}]^{3+}$	14.2 (8.4)	−81.6 (−44.8)
Prod 2	$[L'Cu^{I}]^{+} + [H_4L']^{2+} + [Cu^{I}(NCMe)_4]^{2+}$	−167.7 (−66.8)	−76.7 (−16.0)

[a] Free energies are included in parentheses.

in an increase of the $Cu-N_4$ bond length compared to the reactant. Comparison of Mulliken spin density analysis suggests that the copper center is closer to Cu^{II} than Cu^{I}. This means that the internal electron transfer step has not yet occurred.

A second complex is protonated at N_1 to form $[H_3L'Cu^{II}]^{3+}$. Upon protonation the N donor dissociates from the metal center ($Cu-N_1$ bond length of 4.852 Å), and its place is taken by a counter-ion. The remaining Cu−N bonds show an overall shortening compared to the reactant. The third counter-ion is non-bonding. As for the reactant and $[HL'Cu^{II}]^{+}$, the complex has a d^9 Cu center with a doublet ground state.

The calculated structure for Intermediate sets 1 and 2 are broadly similar in that the ligand is tetra-coordinate for complex $[HL'Cu]^{n+}$ and tricoordinate for $[H_3L'Cu^{I}]^{n+}$. Although the ligand coordination is similar, the change in oxidation number and charge results in a change in coordination number overall. For $[HL'Cu]^{2+}$ a second counter-ion binds to the metal center, giving the complex a roughly octahedral coordination geometry overall. $[HL'Cu]^{2+}$ has a triplet ground state, and Mulliken spin density analysis shows that the Cu center in this complex is closer to Cu^{II} than Cu^{III}, so the complex is best described as Cu^{II} with an oxidized ligand. Molecular orbital analysis shows that the electron comes from an orbital centered on N_1. Therefore the bonding between N_1 and the Cu center can be described as shown in Figure 7 with the electron coming from the non-bonding lone pair on nitrogen. Since the ligand is no longer negatively charged the $Cu-N_1$ bond is not as ionic as that in $[HL'Cu^{II}]^{+}$. As a consequence it is similar in length to that of the reactant. The second complex in Intermediate set 2, $[H_3L'Cu^{I}]^{2+}$, has a singlet ground state and shows a reduction of coordination number from five to four, which is consistent with the change from Cu^{II} to Cu^{I}.

In Products 1 both copper complexes have formally Cu^{I} centers and singlet-ground states. For $[H_4L'Cu^{I}]^{3+}$, the second ligand arm dissociates from the metal center upon protonation to give structure (g). Acetonitrile has a strong affinity[15] for Cu^{I} and when included in the model displaces the counter-ion. The ligand then dissociates to form $[Cu(MeCN)_4]^{+}$ and the free ligand, $[H_4L']^{2+}$. The calculated N_1-C_1 distance of the imine $[Cu^{I}L']^{+}$ product is consistent with the formation of a N−C double bond and in good agreement with experiment. As discussed previously,[18] counter-binding for this species is weak, and so the counter-ion has been excluded from the calculation.

Calculated Energies. As emphasized earlier, the three reaction pathways pass through only two sets of intermediates, Intermediate set 1 and Intermediate set 2. The relative energies of reactants, Intermediate sets 1 and 2, and products are presented in Table 2, both with and without the counter-ions.

The overall amine to imine oxidation reaction is calculated to be exothermic by 77 kJ mol^{-1} (with the counter-ion). Proton transfer between reactants to form Intermediate set 1 was calculated to be endothermic by only 18.6 kJ mol^{-1}. In comparison Intermediate set 2 lies 121.1 kJ mol^{-1} above the reactants in energy, significantly disfavoring reaction pathways 2 and 3. The destabilization of Intermediate set 2 compared to Intermediate set 1 can be at least partially attributed to the high energy intermediate $[HL'Cu^{II}]^{2+}$, in which the ligand has been oxidized.

The large difference in energy between Intermediate sets 1 and 2 suggest that the two step Pathway 1 is preferred where the electron and second proton are transferred together as a hydrogen atom, rather than individual steps as has been described for other systems. Furthermore, the electronic structure analysis of Intermediates 1 suggests that at this point in the reaction the internal electron transfer has not yet occurred. Instead it must take place in the final step, with hydrogen transfer, as represented in Figure 6.

Table 3. Calculated Energies of Proton Transfer for Model 1 Including Counter-ions, Where $MH^+ = [H_2L'Cu^{II}]^{2+}$

	ΔE (kJ/mol)
shuttle (S)	(a) $MH^+ + S \rightarrow M + SH^+$
triflate	154.8
ether	140.0
water	177.5

It is also important to mention the importance of the counter-ion in the reaction profile. Table 2 presents the relative energies of the species along the reaction pathway both with and without counter-ions. In all but the final product it plays an active role, binding directly to the metal centers. In comparison, the solvent binds more weakly except to the final products, where acetonitrile has a strong affinity for the Cu^I centers. Since counter-ion binding is found to be favorable except for the products, it leads to a decrease in the exothermicity of the reaction from -167.7 to -76.7 kJ mol^{-1}. The counter-ion also significantly stabilizes Intermediate set 1 relative to Intermediate set 2 which can be attributed to the balancing of the +3 and +1 charges of the complexes in the former. Therefore it is imperative to include the counter-ions to correctly describe this system.

Mechanism in More Detail: Proton Shuttling. Pathway 1 was explored in more detail to estimate energetic barriers to the reaction. For the transfer steps there are two probable mechanisms: (1) shuttling via a third species in the reaction mixture, or (2) transfer directly between complexes. Both are explored below.

There are several species in the reaction mixture which may be capable of acting as a shuttle. These include ether, the counter-ion (triflate) and possible traces of water. The energy of proton transfer to the shuttle was calculated for the first step of pathway 1 for shuttles S = ether, triflate, and water and are presented in Table 3 where transfer 1 occurs between Reactants (Rx) to form Intermediate set 1 (Int 1) and transfer 2 between the Intermediate set 2 (Int 2) to form the products (Prod 1).

As shown, proton transfer from the reactant to the shuttle, S, (transfer 1) is calculated to be endothermic by at least 140 kJ mol^{-1} for the three shuttles studied. The energy associated with hydrogen and electron shuttling was also calculated, but both hydrogen and electron transfers were calculated to give high energy or unstable intermediates. For hydrogen shuttling, O−H or C−S bond cleavage occurred in all cases.

Mechanism in More Detail: Proton and Electron Transfer Directly between Complexes. Since proton transfer via a shuttling mechanism was calculated to be energetically costly, we next explored transfer directly between the complexes. For this system, calculating the transition state is not realistic because of its size and the number of possible conformations. Instead, to estimate the barrier to proton or hydrogen transfer between complexes, we carried out scans varying the relevant N−H or C−H distance as shown in Figure 8. In principle these calculations do not distinguish between proton or hydrogen atom transfer as the electronic state of the individual complexes is not defined, but the difference in energy between Intermediate sets 1 and 2 make it possible to identify which process is occurring. As it is prohibitively

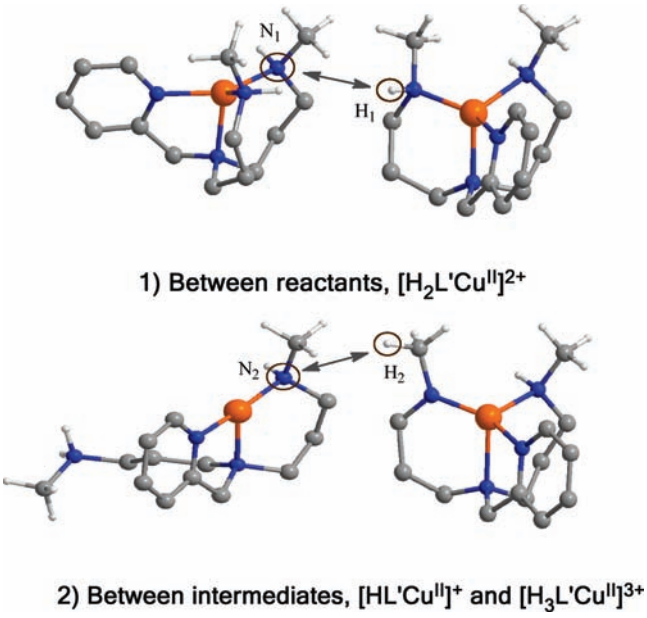

Figure 8. Scans were carried out varying the N−H distances shown above. Counter-ions are not shown for purposes of clarity.

Table 4. Estimated Barriers for Transfer Steps[a]

transfer step	transfer type	r(N−H) at E(max)/Å	E(max)/ kJ mol^{-1}
$2\,[H_2L'Cu^{II}]^{2+} \rightarrow [HL'Cu^{II}]^{+} + [H_3L'Cu^{II}]^{3+}$	H^+	1.2	89.1
$[HL'Cu^{II}]^{+} + [H_3L'Cu^{II}]^{3+} \rightarrow [L'Cu^{I}]^{+} + [H_4L'Cu^{I}]^{3+}$	H	1.7	134.5

[a] Note: These values are not corrected for zero-point energy because of the size of the system.

time-consuming to explore all possibilities for systems of this size, several reasonable conformations were chosen for each point along the scan. The calculated values then represent the upper bound in energy for the transfer steps rather than precise barriers or transition states (Table 4). Various options for treatment of the charges were explored to try and reduce computational effort, including MM charges or the ONIOM methodology; however, the results were found to differ significantly from those calculated with DFT, particularly in the case of MM charges.

The first transfer step occurs between the reactants to form Intermediate set 1. The barrier to transfer was estimated via a scan of the N−H bond distance shown in part (1) of Figure 8. ONIOM calculations with the carbon atoms of the chelate rings in the MM region were used to preoptimize structures, and then the geometries were reoptimized with DFT for the highest energy points. Both ONIOM and DFT results are presented in Figure 9. Single point calculations with BS II and solvent corrections were then carried out for the highest point and those immediately adjacent to it.

Along the DFT curve, the barrier to transfer is calculated to be 38 kJ mol^{-1} at a N−H distance of 1.2 Å. This increases to 89.1 kJ mol^{-1} for BS II including solvent corrections. Since this is lower in energy than Intermediate set 2 (121 kJ mol^{-1}), this process is clearly proton and not hydrogen transfer. The change in energy with basis set

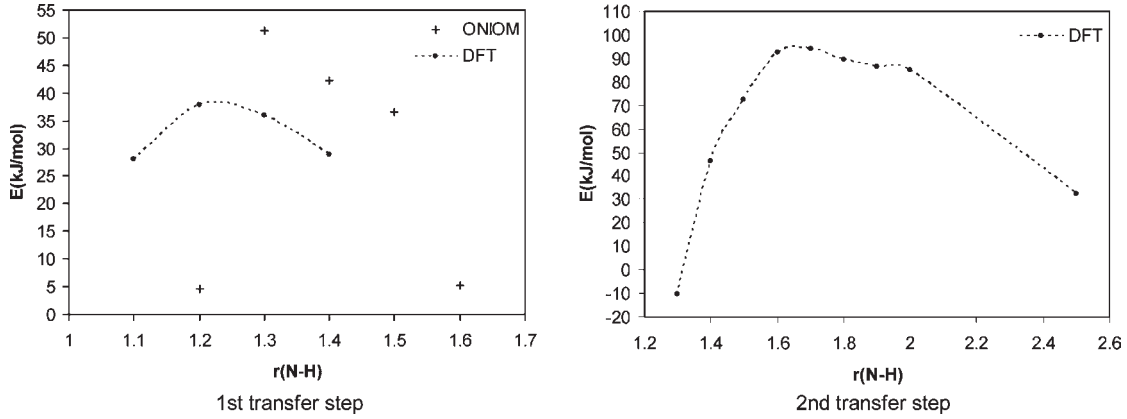

Figure 9. Scan results for the first and second transfer steps.

and solvent corrections is large compared to that calculated for Intermediate set 1 (12 kJ mol^{-1}). However, even if the barrier is overestimated these results demonstrate that proton transfer directly between the complexes is favorable.

During the transfer, even at the relatively long N−H distance of 1.6 Å, the N donor N_1 in Figure 8 dissociates from the copper center. This is probably not surprising as the Cu-amine bond is known to be labile in solution[15] and the N_1 donor is not coordinated in $[H_3L'Cu^{II}]^{3+}$ or $[H_3L'Cu^{I}]^{2+}$. Importantly, the dissociation of the ligand arm allows the copper centers to move further apart, reducing the Coulombic repulsion.

The hydrogen transfer from Intermediate set 1 to form Products 1, transfer 2, was explored through a scan of the N−H distance shown in part (2) of Figure 8. This reaction is more challenging as it involves hydrogen transfer and an internal electron transfer in $[HL'Cu^{II}]^{+}$ from the ligand to the Cu center. The DFT optimized scan results are presented in Figure 9. More points along the scan were calculated compared to the first transfer step because of the complexity of the reaction.

During this second transfer, as the $HL'Cu^{III}$ and $H_3L'Cu^{I}$ complexes approach, the two d^9 copper centers couple to give an antiferromagnetic singlet overall, with the ferromagnetically coupled triplet lying higher in energy. This magnetic supramolecular coupling through hydrogen bonding is a phenomenon that has also been observed experimentally in related systems.[34,35]

At shorter N−H distances, about 1.5 Å, this "open-shell" singlet collapses into the closed shell singlet which characterizes the product. As in the first scan, the N donor receiving the proton, N_2, dissociates from the metal center, this time at an N−H distance of 2.0 Å, giving the slight hump in the graph around this point. Ligand dissociation is more endothermic for $[H_3L'Cu^{II}]^{2+}$ than for the reactant, and this increases the height of the barrier.

The estimated barrier for transfer with BS II and solvent corrections is 135 kJ mol^{-1} relative to reactants, which is slightly higher in energy than Intermediate set 2, but as this is an upper bound for the energy based on a limited number of conformations we expect the real value to be lower. Zero-point energy corrections should further reduce the barrier since they stabilize the intermediates relative to reactants by between 8 and 14 kJ mol^{-1} (see note in Experimental Section). Since the formation of Intermediate set 2 is likely to have a sizable barrier, Pathways 2 and 3 are unlikely to be competitive.

In summary, on the basis of these results we predict a two step mechanism, Pathway 1, where the first step is proton transfer directly between the reactants over a maximum barrier of 89 kJ mol^{-1} to give Intermediate set 1, which lies 18.6 kJ mol^{-1} above the reactants in energy. The next step is hydrogen transfer, again directly between the complexes, over a barrier of approximately 135 kJ mol^{-1}, reducing the Cu^{II} of the second complex to Cu^{I}. Also during this step, the Cu^{II} center of $[HL'Cu^{II}]^{+}$ is reduced by the ligand to Cu^{I} via an internal electron transfer process. Overall the ligand loses two protons and two electrons. The final step is displacement of the ligands and counter-ions from the copper center by the solvent to give the final products, $[L'Cu^{I}]^{+}+[H_4L']^{2+}+[Cu^{I}(NCMe)_4]^{2+}$. The pathway proposed here is thus a proton transfer followed by hydrogen transfer (one electron and one proton). It may be related to the hydride transfer processes that have experimental precedent both in chemical[36] and in biological systems.[37]

Conclusions

The amine to imine oxidation reaction reported recently has been studied using a mononuclear model. Pathways involving individual and concerted proton and electron transfer steps were explored.

We predict a two step mechanism with proton transfer as the first step and then a second step where an electron and second proton are transferred together. At the same time the ligand is oxidized a second time, reducing the copper center to which it is bound. The overall barrier to the reaction was calculated to be at most 135 kJ mol^{-1}, although we expect the real barrier to be somewhat lower in energy. The final step in the reaction is displacement of the ligands and counterions from the copper center by the solvent to give the final products, $[L'Cu^{I}]^{+}+[H_4L']^{2+}+[Cu^{I}(NCMe)_4]^{2+}$. Other

(34) Bertrand, J. A.; Black, T. D.; Eller, P. G.; Helm, F. T.; Mahmood, R. *Inorg. Chem.* **1976**, *15*, 2965–2970.
(35) Ray, M. S.; Ghosh, A.; Chaudhuri, S.; Drew, M. G. B.; Ribas, J. *Eur. J. Inorg. Chem.* **2004**, 3110–3117.
(36) Fukuzumi, S.; Fujioka, N.; Kotani, H.; Ohkubo, K.; Lee, Y.-M.; Nam, W. *J. Am. Chem. Soc.* **2009**, *131*, 17127–17134.
(37) Nagel, Z. D.; Klinman, J. P. *Chem. Rev.* **2006**, *106*, 3095–3118.

pathways were excluded based on the high energy of intermediates.

This reaction differs from the usually accepted three or four step pathways for transition metal catalyzed amine to imine oxidation in which the protons and electrons are transferred in individual steps. Furthermore, the second step of the reaction is predicted to be complex, with two electrons and a proton transferred simultaneously.

The reason why this reaction occurs only for this particular complex is likely related to the combination of steric and electronic effects provided by the ligand to the copper coordination sphere, and could only be fully ascertained by joint experimental and theoretical studies on similar complexes that did not present this reactivity.

Acknowledgment. We gratefully acknowledge the Spanish MICINN (Consolider Ingenio 2010 Grant CSD 2006-0003 and Grants CTQ2007-67918, CTQ2008-06866-CO2-02) and the ICIQ Foundation for financial support.

Supporting Information Available: Cartesian coordinates for computed geometries and functional testing. This material is available free of charge via the Internet at http://pubs.acs.org.